# Simulation of microtearing turbulence in national spherical torus experiment[a)]

W. Guttenfelder,[1,b)] J. Candy,[2] S. M. Kaye,[1] W. M. Nevins,[3] E. Wang,[3] J. Zhang,[4] R. E. Bell,[1] N. A. Crocker,[4] G. W. Hammett,[1] B. P. LeBlanc,[1] D. R. Mikkelsen,[1] Y. Ren,[1] and H. Yuh[5]
[1]*Princeton Plasma Physics Laboratory, Princeton New Jersey 08543, USA*
[2]*General Atomics, San Diego, California 92186, USA*
[3]*Lawrence Livermore National Laboratory, Livermore, California 04551, USA*
[4]*University of California Los Angeles, California 90095, USA*
[5]*Nova Photonics Inc., Princeton, New Jersey 08540, USA*

(Received 23 December 2011; accepted 6 February 2012; published online 27 April 2012)

Thermal energy confinement times in National Spherical Torus Experiment (NSTX) dimensionless parameter scans increase with decreasing collisionality. While ion thermal transport is neoclassical, the source of anomalous electron thermal transport in these discharges remains unclear, leading to considerable uncertainty when extrapolating to future spherical tokamak (ST) devices at much lower collisionality. Linear gyrokinetic simulations find microtearing modes to be unstable in high collisionality discharges. First non-linear gyrokinetic simulations of microtearing turbulence in NSTX show they can yield experimental levels of transport. Magnetic flutter is responsible for almost all the transport (~98%), perturbed field line trajectories are globally stochastic, and a test particle stochastic transport model agrees to within 25% of the simulated transport. Most significantly, microtearing transport is predicted to increase with electron collisionality, consistent with the observed NSTX confinement scaling. While this suggests microtearing modes may be the source of electron thermal transport, the predictions are also very sensitive to electron temperature gradient, indicating the scaling of the instability threshold is important. In addition, microtearing turbulence is susceptible to suppression via sheared $E \times B$ flows as experimental values of $E \times B$ shear (comparable to the linear growth rates) dramatically reduce the transport below experimental values. Refinements in numerical resolution and physics model assumptions are expected to minimize the apparent discrepancy. In cases where the predicted transport is strong, calculations suggest that a proposed polarimetry diagnostic may be sensitive to the magnetic perturbations associated with the unique structure of microtearing turbulence. © *2012 American Institute of Physics*. [http://dx.doi.org/10.1063/1.3694104]

## I. INTRODUCTION

Microtearing instabilities have been predicted to be unstable in spherical tokamaks (STs),[1–11] conventional aspect ratio tokamaks,[12,13] and reverse field pinches.[14] The stability characteristics and predicted level of transport are, therefore, of broad interest to the magnetic fusion community. By microtearing, we refer to resonant electromagnetic modes with tearing parity (flux-surface averaged $\langle A_{||} \rangle$ is finite) on a rational flux surface, $q = m/n$, (where q is the safety factor) at high toroidal (n) and poloidal (m) mode number that are stable to conventional resistive tearing instability.[15,16] Because of the strong stabilizing influence of field line bending (represented by a large negative tearing parameter that asymptotes to $\Delta' = -2m/r$ at high m (Ref. 17)), some other mechanism must be responsible for instability, such as the time-dependent thermal force[18–28] or trapped-passing particle interaction.[29–31] Either mechanism requires finite electron collisionality ($\nu_e$) as well as sufficient electron temperature gradient ($\nabla T_e$) and electron beta ($\beta_e$) for instability to ensue.

Significant microtearing induced transport is expected to occur if many small scale islands grow sufficiently wide to overlap and destroy flux surfaces such that electrons diffuse in a region of stochastic field lines. In the cylindrical limit, a single resonant mode can reconnect[17] and cause a magnetic island of width $w_{island} = 4\sqrt{\delta B/B_0 \cdot rR/ns}$ to form, where $B_0$ is the equilibrium field strength, R(r) is the major (minor) radius, and $s = r/q \cdot q'$ is the magnetic shear. If the single-mode island width becomes larger than the separation between rational surfaces, $\Delta r_{rat} = 1/nq' = 1/k_\theta s$ ($k_\theta = nq/r$), stochasticity is expected to develop[32] which can cause rapid transport of electrons following the perturbed fieldline trajectories.[33] If many toroidal modes are present (separated by $\Delta n$), the minimum distance between adjacent resonant surfaces is $\delta r_{rat} \approx \Delta n/n^2 q'$. Therefore, the island overlap criterion for stochasticity onset ($w_{island} > \delta r_{rat}$) is more easily satisfied, especially for higher n.

Evaluating this condition and estimating transport requires the amplitude of the saturated $\delta B/B$ perturbations. The quasi-linear approximation $\delta B/B \approx \rho_e/L_{Te}$ (derived from nonlinear theory for a shear-free slab,[20] with similar forms found in sheared slab theories[24,28]) was used along with collisional and collisionless test-particle stochastic transport models[33] to model single NSTX[34,35] and RFX[14] discharges with some quantitative agreement. However, the stochastic $\chi_e$ models do not follow the predicted scaling of the linear instability. Overall, it is unknown how the transport will scale from first

[a)]Paper TI2 6, Bull. Am. Phys. Soc. **56**, 280 (2011).
[b)]Invited speaker.

 

principles turbulence simulations, which motivates the work in this paper.

Of particular interest to spherical tokamaks is the scaling with collisionality. Dedicated dimensionless scaling studies in both NSTX[36–38] and Mega-Ampere Spherical Tokamak (MAST)[39,40] find that the normalized energy confinement time exhibits a strong inverse scaling with collisionality, $(\Omega\tau_E) \sim \nu_{*e}{}^{-(0.8-0.95)}$. This scaling predicts improved confinement at smaller values of $\nu_*$ envisioned for next generation STs.[41,42] It is important to clarify the cause of this scaling and whether it will hold at lower $\nu_*$.[43] In many of these discharges, the microtearing mode has been predicted to be unstable, and over a particular range of collisionality (roughly characterized by $\nu_e/\omega < 1$, or weakly collisional), the linear growth rates decrease with decreasing $\nu_e$, qualitatively consistent with the observed confinement scaling. This dependence is opposite to that expected for traditional electrostatic ion temperature gradient and trapped electron modes (ITG/TEMs), where increasing $\nu_e$ has a stabilizing influence by detrapping the trapped electrons which otherwise tend to enhance growth rates. Because of this unique dependence on $\nu_e$, it is thought the microtearing mode may be an important transport component in at least some ST discharges.

First attempts at non-linear microtearing gyrokinetic simulations[44] using the GS2 code[45,46] based on MAST parameters found the simulations ultimately lead to numerical instability with much of the energy accumulating (non-physically) in the smallest radial scales (highest $k_x$ modes). A thorough discussion of the issues encountered, including resolution issues and numerical constraints is provided in Ref. 44. A single gyrofluid microtearing simulation has also previously been reported,[47] but with little discussion of the resulting turbulence characteristics and transport dependencies.

More recently, the first successful non-linear gyrokinetic simulations have been reported for parameters based on NSTX experimental data[48] and for higher aspect ratio parameters based on ASDEX-UG.[49] The NSTX simulations are performed for a plasma in which the ion thermal transport is well described by neoclassical theory and other instabilities such as ETG appear to be stable, so microtearing turbulence is expected to play a significant role in energy confinement. In this paper, we describe additional nonlinear simulations that vary electron beta, collisionality, and $E \times B$ shear around the nominal experimental values to determine the scaling of the nonlinear transport. Most notably, the simulations predict a near linear scaling of electron thermal transport with $\nu_e$, roughly consistent with the global confinement scaling. We also present additional details of the unique microtearing turbulence characteristics predicted in NSTX, which are used to motivate possible experimental measurements.

The remainder of this paper is organized as follows. Section II provides details of the experimental NSTX discharge, linear stability analysis, and model assumptions. Section III presents the baseline non-linear simulations, discussing resolution requirements, spectral characteristics, and stochasticity. Section IV then shows how the simulated microtearing transport scales with collisionality, temperature gradient, beta, and $E \times B$ shear. To address the possibility of measuring microtearing turbulence, in Sec. V, we investigate the real space structure of the density and magnetic field perturbations. We conclude with a summary in Sec. VI.

## II. EXPERIMENTAL PARAMETERS AND LINEAR ANALYSIS

The Eulerian gyrokinetic code GYRO (Refs. 50–53) is used for both linear and non-linear simulations which are based on a high collisionality NSTX discharge that is part of energy confinement scaling studies[36,37] ($B_T = 0.35$ T, $I_p = 0.7$ MA, R/a = 0.82/0.62 m, $P_{NBI} = 4$ MW, line-averaged density $\bar{n}_e = 5.4 \times 10^{19}\,m^{-3}$, peak temperatures $T_e(0) \approx T_i(0) = 0.85$ keV, volume-averaged toroidal beta $\beta_{tor} = 19\%$). Many of the properties of the linear microtearing mode and scaling for this case are described in Ref. 11. Table I lists the local experimental parameters used in the simulations for the single location r/a = 0.6 investigated in this paper. The local electron beta is defined as $\beta_e = 8\pi n_e T_e / B_T^2$ using the vacuum value $B_T = 0.35$ T, while $\beta_{e,unit}$ is defined replacing $B_T$ with the quantity $B_{unit} = B_T \cdot \rho/r \cdot d\rho/dr$ [r is a near mid-plane minor radius,[52] $\rho = (\Psi_t/\pi B_T)^{1/2}$, $\Psi_t$ is the toroidal flux] as used in normalizations throughout GYRO. The collision frequency coefficient is $\nu_{ei} = 4\pi n_e e^4 \log\Lambda / (2T_e)^{3/2} m_e^{1/2}$. Parameters related to the flow are the Mach number $Ma = v_{Tor}/c_s = R\omega_0/c_s$, the $E \times B$ shearing rate $\gamma_E = -r/q \cdot \partial\omega_0/\partial r$, and the rotation shearing rate $\gamma_P = R \cdot \partial\omega_0/\partial r = (qR/r) \cdot \gamma_E$, where $\omega_0 = -d\Phi_0/d\psi$ is the toroidal rotation frequency, $\Phi_0$ is the equilibrium electric field potential and $\psi$ is the poloidal flux (assuming no other contribution to $E_r$ from diamagnetic or poloidal flows, which is appropriate for the core of most NSTX NBI plasmas). Other normalizing quantities are the minor radius, a = 0.62 m, sound speed $c_s = (T_e/m_d)^{1/2}$, and deuterium ion gyroradius $\rho_{s,D} = (m_d \cdot T_e)^{1/2}/B_{unit}$ evaluated at the local electron temperature ($T_e = 0.45$ keV).

The simulations below include most physical effects expected to be important in the NBI heated NSTX discharges, including kinetic electrons and deuterium ions at full mass ratio ($m_i/m_e = 3600$), shear magnetic perturbations ($\delta B = \nabla \times \delta A_{||}$), and electron pitch angle scattering. Geometric quantities are derived from experimentally constrained numerical equilibrium reconstruction. Although expected to be important, toroidal flow and flow shear are not included unless otherwise noted.

TABLE I. Parameters for NSTX discharge 120968, t = 0.560 s at r/a = 0.6.

| r/a | q | s | $T_e/T_i$ | $a/L_{Te}$ | $a/L_{Ti}$ | $a/L_{ne}$ | $a/L_{nd}$ | $\beta_e$ (%) | $\beta_{e,unit}$ (%) | $\nu_{ei}$ ($c_s/a$) | $Z_{eff}$ | $\gamma_E$ ($c_s/a$) | $\gamma_P$ ($c_s/a$) | Ma |
|---|---|---|---|---|---|---|---|---|---|---|---|---|---|---|
| 0.6 | 1.69 | 1.74 | 1.05 | 2.72 | 2.36 | −0.83 | 0.35 | 8.84 | 2.45 | 1.45 | 2.92 | 0.17 | 0.74 | 0.22 |

To minimize computational expense for first nonlinear simulations, compressional magnetic perturbations ($\delta B_{||}$) are ignored since they do not affect the microtearing mode.[5,11] In addition, only one kinetic ion species (deuterium) is kept. As shown in linear analysis,[11] finite impurity content ($Z_{eff}=2.9$ from carbon profile measurements) can provide a destabilizing influence to the microtearing mode through both the electron-ion collisionality dependence as well as through shielding the electrostatic potential response via the nearly adiabatic ion response ($\delta n_i/n_i \approx -Z_{eff,poisson}\cdot\delta\varphi/T_i$). Numerically, there is no additional expense by including the effect of $Z_{eff}>1$ in the pitch-angle scattering collision operator which has an energy-dependent coefficient proportional to $\nu_{ei}\cdot[Z_{eff}+H(v)]/v^3$, where $H(v)=\exp(-v^2)/\pi^{1/2}v+(1-1/2v^2)\,\mathrm{erf}(v)$ and $v=v_e/v_{th,e}$. As shown in Fig. 1, neglecting a dynamic impurity species (D only, so that $Z_{eff,poisson}=1$) leads to a maximum growth rate that is ~15% smaller than the calculation with two ion species (D+C, $Z_{eff,poisson}=2.9$), and the width of the unstable spectra is smaller. In both cases, $Z_{eff}=2.9$ is used in the collision operator.

The linear microtearing instability depends explicitly on the presence of resonant parallel current layers ($\delta j_{||}$) centered on the rational surfaces. As an example, Fig. 2(a) shows the radial variation of the real component of the parallel current for the most unstable mode ($k_\theta\rho_s=0.63$, $n=30$), taken at a snapshot in time at the outboard midplane ($\theta=0$). The current channel is centered on the $q=51/30=1.7$ rational surface with a width $\Delta_j\approx 0.3\ \rho_s$ (≈1.4 mm) or ~1/3 of the rational surface separation $\Delta r_{rat}=0.9\ \rho_s$. As a result of the narrow current channel, fine radial resolution ($\Delta x\approx 0.03\ \rho_s$) is required to obtain quantitative convergence in the linear growth rate.

It is computationally prohibitive (and typically unnecessary) to use such high resolution in a non-linear turbulence simulation. However, the radial resolution must at minimum be able to distinguish the separation in rational surfaces of the most unstable modes in the simulation domain (or possibly even the largest value of $k_\theta$) if the microtearing physics is to be properly represented. Considering the finite difference scheme used in GYRO,[51] a minimum resolution criterion would be four grid points per rational surface or

$$\Delta x < \min\left(\Delta r_{rat}\right)/4 \;=\; 1/\left(4k_{\theta,\max}s\right). \qquad (1)$$

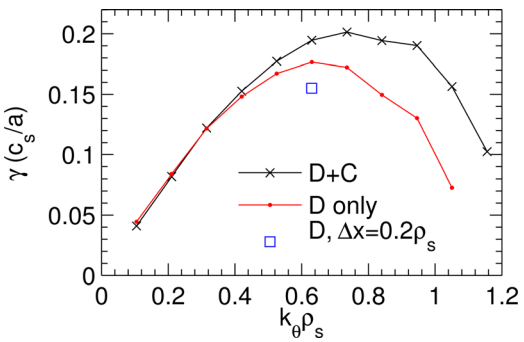


FIG. 1. (Color online) Linear growth rate spectra at $r/a=0.6$ using deuterium and carbon and deuterium only. Also shown is the linear growth rate of the $n=30$ ($k_\theta\rho_s=0.63$) mode using the exact same grid parameters as the non-linear simulations below ($L_x=80\rho_s$, $nx=400$, $\Delta x=0.2\rho_s$).

In the present case ($n=30$), this is satisfied for $\Delta x\approx 0.2\ \rho_s$.

To verify the microtearing mode is in fact represented with such resolution, an additional *linear* simulation is performed using the same numerical domain as the nonlinear simulations below ($\Delta x=0.2\ \rho_s$, $L_x=80\ \rho_s$, $nx=400$) instead of the standard flux-tube domain ($\Delta x=0.03\ \rho_s$, $L_x=\Delta r_{rat}=0.9\ \rho_s$, $nx=32$). Fig. 2(b) shows there is still a distinct current layer associated with each rational surface, although the fine scale features of $\delta j_{||}(r)$ are no longer represented. (Note the abscissa in Fig. 2(b) is scaled to show only three rational surfaces, although there are 88 total in the simulation domain for the $n=30$ mode.) The consequence of the sub-optimal resolution in this case is a linear growth rate that is ~12% smaller (shown by the blue square in Fig. 1) than the quantitatively converged high resolution case. Nevertheless, the structure and scaling of the microtearing mode is similar to the flux-tube case. As the grid spacing is increased to $\Delta x=0.4$ or $0.8\ \rho_s$ ($nx=200,100$) individual rational surfaces are no longer distinguishable and the resulting instability takes on a completely different (non-physical) appearance with a growth rate that eventually increases dramatically ($\gamma=0.20, 0.40\ c_s/a$).

If Eq. (1) must always be satisfied, it severely restricts the parameter range that practically can be simulated as larger magnetic shear further out in radius will require yet smaller $\Delta x$. At present, it is unclear if this will always be the case or if additional effects will take over non-linearly.

## III. NON-LINEAR SIMULATIONS

### A. Numerical grids

Nonlinear simulations use the same parameters discussed above and outlined in Table I. The simulations are run in the

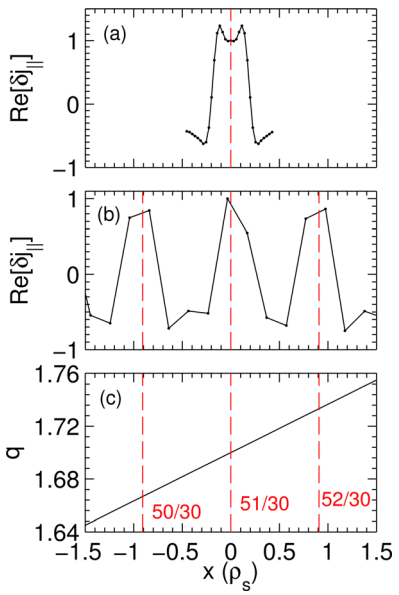


FIG. 2. (Color online) Radial variation of parallel current perturbations from linear simulations at $\theta=0$ for two different perpendicular resolutions: (a) $\Delta x=0.03\ \rho_s$ ($L_x=0.9\ \rho_s$, $nx=32$) (typical flux-tube domain), (b) $\Delta x=0.2\ \rho_s$ ($L_x=80\ \rho_s$, $nx=400$) (similar domain as non-linear simulations). (c) The q profile used in each simulation. Dashed lines are located at each rational surface associated with the $n=30$ ($k_\theta\rho_s=0.63$) mode.

TABLE II. Numerical grid parameters for the non-linear simulations.

| Case | $L_x \times L_y$ ($\rho_s$) | $n_x \times n_y$ | $\Delta x$ ($\rho_s$) | $\Delta t$ ($a/c_s$) | $n_E \times n_\lambda \times n_\tau$ ($\times s_{v\|\|}$) | cpu-hrs |
|---|---|---|---|---|---|---|
| R1 | $80 \times 60$ | $400 \times 8$ | 0.2 | 0.002 | $8 \times 12 \times 14$ ($\times 2$) | ~100,000 |
| R2 | $80 \times 100$ | $540 \times 16$ | 0.15 | 0.001-0.0015 | $8 \times 12 \times 14$ ($\times 2$) | ~250,000 |

*local* limit (i.e., no equilibrium profile variations) with a domain width chosen to be $L_x = 80\ \rho_s$. Fixed boundary conditions are enforced for all simulations to most naturally include equilibrium flow shear when desired. Damped buffer regions of width $\Delta^b = 8\ \rho_s$ and damping rate $\nu^b = 1\ c_s/a$ are used at both radial boundaries to prevent profile relaxation[53] and the time- and flux-surface-averaged gradient contribution from the $n = 0$ zonal moments is less than 1% of the equilibrium values.

Two binormal grids were used to test for convergence, $L_y = 60\ \rho_s$ and $100\ \rho_s$, corresponding to a separation in toroidal mode numbers of $\Delta n = 5$ and 3. Using 8 and 16 spectral modes the maximum toroidal mode numbers correspond to $n = 35$ and 45, respectively. The radial resolution requirement discussed previously was satisfied by using 400 and 540 radial grid points, giving $\Delta x = 0.2\ \rho_s$ and $0.15\ \rho_s$. Velocity space and parallel orbit grids were the same as determined from extensive linear convergence studies (8 energies, 12 pitch angles and 14 parallel orbit mesh points, $\times 2$ signs of parallel velocity). Time steps between $0.001-0.002\ a/c_s$ were used to satisfy integration stability requirements. Table II summarizes the relevant parameters. The simulations required multiple 12–24 hr restarts using 768–1536 cores on either the NERSC Franklin Cray XT4 or the ORNL Jaguar Cray XT5 to achieve statistical stationarity, expending ~100,000 (~250,000) cpu-hrs for the R1 (R2) grid.

## B. Time series

Time traces of the resulting electron thermal diffusivity are shown in Fig. 3 for the two grid resolutions up to 600 and 900 $a/c_s$. Each simulation has run for ~0.5 M time steps with no sign of spurious growing modes at high-$k_\perp$. The time-averaged transport in each case is $\chi_e = 1.2\rho_s^2 c_s/a$ and $1.5\rho_s^2 c_s/a$, corresponding to 6 and 7.25 $m^2/s$. These values fall within the range of the local experimental values 5–8 $m^2/s$ determined using TRANSP,[54] illustrating microtearing turbulence can indeed drive relevant levels of electron thermal transport in NSTX plasmas.

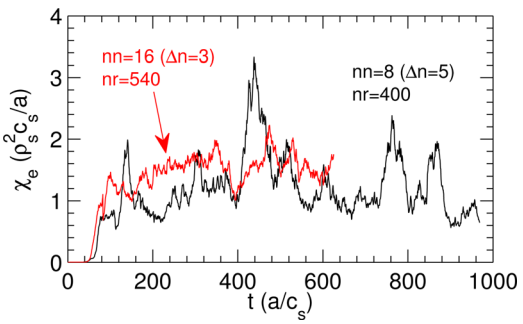


FIG. 3. (Color online) Time series of electron thermal diffusivity for two different grids.

A unique feature of these simulations is that nearly all of the electron thermal transport (~98%) comes from the magnetic flutter contribution ($\sim v_{||,e} \cdot \delta B_r/B$) in contrast to ITG/TEM turbulence, ETG turbulence, or even simulations that approach the ideal or kinetic ballooning mode limit ($\chi_{e,em}/\chi_{e,tot} \sim 50\%$).[55–58] In addition, there is negligible particle, ion thermal or momentum transport, consistent with strong magnetic flutter contribution and the fact that ions are much heavier than electrons ($v_{||,i} \ll v_{||,e}$).

## C. Spectral properties

An important verification that these simulations are in fact sufficiently resolved radially is shown by the strongly decaying $k_x$ tails of the power spectra for $\delta n$, $\delta A_{||}$, and $\delta j_{||}$ (integrated over $k_\theta$ and time) shown in Figs. 4(a), 4(c), and 4(e) for $\theta = 0$ (black & red solid lines for R1 and R2). (The

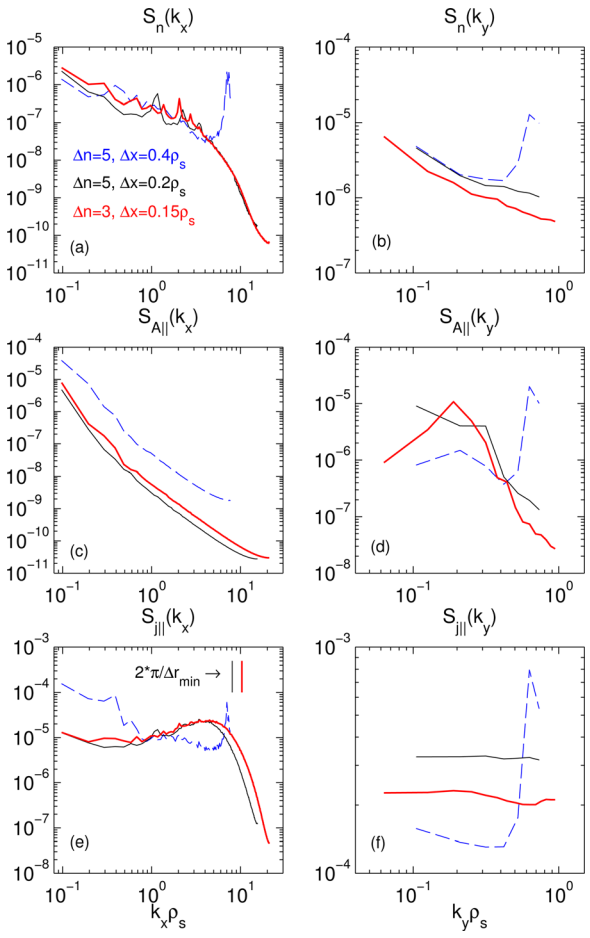


FIG. 4. (Color online) Time-averaged integrated power spectra versus (left) $k_x$ and (right) $k_y$ for (a,b) $\delta n$, (c,d) $\delta A_{||}$, and (e,f) parallel current, $\delta j_{||}$. The three lines represent different resolution parameters. The vertical lines in (e) illustrate the location of the minimum rational surface separation for each numerical grid ($n_{max} = 35$ and 45).

potential spectra are not shown as they are identical to density, consistent with the nearly exact adiabatic ion response, $\delta n/n = -(e\delta\varphi/T)$.[11]) In contrast, the density and parallel current spectra from an insufficiently resolved simulation (blue dashed line) shows a pile-up at the highest $k_x$ modes for both the density and parallel current. This pile-up also occurs at the highest-$k_y$ modes for all quantities as seen in Figs. 4(b), 4(d), and 4(f). To illustrate the resolution criteria discussed above ($k_{x,max} > 2k_{x,rat}$), the vertical lines in Fig. 4(e) show the values of $k_{x,rat} = 2\pi/\Delta r_{min}$ that correspond to the separation in rational surfaces of the highest toroidal mode number in the simulation.

The $\delta n(k_x)$ and $\delta A_{||}(k_x)$ spectra agree very well in the region of spectral decay for the properly resolved simulations. As resolution is refined, the $\delta j_{||}(k_x)$ peak is shifted out and becomes broader, consistent with a narrowing of current layers discussed above in the linear analysis. Above this peak the spectral decay is extremely sharp.

While the $k_y$ spectral range is limited, spectral decay is apparent for both $\delta n$ and $\delta A_{||}$. In the highest resolution case, there is a distinct peak in $\delta A_{||}$ at $k_\theta \rho_s \approx 0.2$ suggesting qualitatively the simulations are not missing larger scale phenomenon that could be important. The discrete peaks in the density $k_x$ spectra ($k_x\rho_s \approx 1-4$, Fig. 4(a)) correspond to the rational surface separation ($k_x = 2\pi/\Delta r_{rat} = 2\pi \cdot s k_\theta$) of the finite $k_\theta$ modes, where the $\delta A_{||}$ spectra peaks (Fig. 4(d)).

The nonlinear frequency spectra of both $\delta n$ and $\delta A_{||}$ (not shown) are centered around the linear dispersion relation which closely follows the electron diamagnetic drift frequency, $\omega \sim \omega_{*e} = k_\theta \rho_s \cdot (a/L_{ne} + a/L_{Te}) \cdot (c_s/a)$. The average spectral width, characterized by the rms value of $\omega$, is $\Delta\omega \approx 0.6\, c_s/a$ indicating a decorrelation time $\tau_d \approx \Delta\omega^{-1} = 1.7\, a/c_s$ or 7 $\mu$s.

The transport due to the electromagnetic perturbations at each $k_\theta$ mode is calculated by $Q_e(k_\theta) = \langle \int d^3v \delta f \cdot 1/2 m v^2 v_{||}\, b \times \nabla A_{||}/B \cdot \nabla r \rangle$, which is roughly proportional to $\sim k_\theta |\delta A_{||}|^2 \sin(\alpha_{A\text{-}f})$, where $\alpha_{A\text{-}f}$ represents a general cross phase between the magnetic perturbations and perturbed distribution function. Consistent with the low-$k_\theta$ peak in $|\delta A_{||}|^2$ (Fig. 4(d)), the transport spectra (Fig. 5) show clearly defined peaks at $k_\theta \rho_s \approx 0.2$–$0.25$ for both grid resolutions giving confidence the simulations are capturing the most important dynamics. In fact, as $\Delta x$ is fixed in the nonlinear simulations,

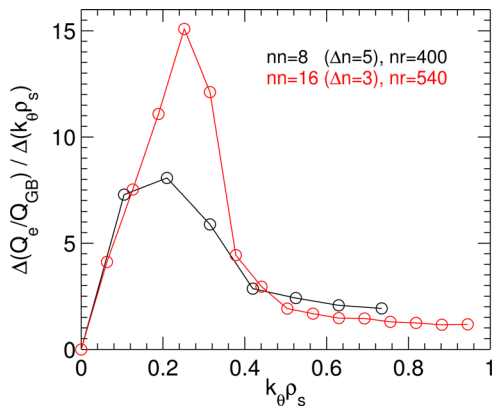


FIG. 5. (Color online) Fractional transport spectra for two resolutions, normalized by wavelength spacing ($\Delta k_\theta \rho_s$).

the ratio $\Delta x/\Delta r_{rat}$ is reduced at lower $k_\theta$ as the spacing between rational surfaces increases, so that lower $k_\theta$ modes are better resolved compared to the modes near $k_{\theta,max}$ (Fig. 2). Since the transport peaks around these modes ($k_\theta \rho_s \sim 0.2$), the present $\Delta x$ resolution may be sufficient.

Comparing Figs. 4(d) and 5 with Fig. 1, we see the nonlinear $k_\theta$ spectral peak is downshifted significantly from the maximum linear growth rate, as predicted to occur in analytic non-linear theory.[20,24,28] From the non-linear electromagnetic term, the nonlinear growth/damping rate for a mode k is proportional to $\gamma_{k,NL} \sim -\sum_{k'} |k \cdot \delta B_{k'}|^2 \cdot \frac{k_\theta - k'_\theta}{k_\theta + k'_\theta}$ (e.g., Ref. 20), where a net positive value of $\gamma_{k,NL}$ implies mode k is absorbing energy (i.e., being driven non-linearly). In the limit of $k_\theta' > k_\theta$, $\gamma_{k,NL} \sim +|k \cdot \delta B_{k'}|^2$ (or $\gamma_{k,NL} \sim -|k \cdot \delta B_{k'}|^2$ for $k_\theta' < k_\theta$), which indicates a preference for energy to transfer from fast growing short wavelength modes (high $k_\theta'$) to long wavelength modes (low $k_\theta$), where damping must occur to achieve a statistical steady state. While the spectrum of modes shown in Fig. 1 are all unstable and would therefore provide no damping at low $k_\theta$, there are likely to be many damped eigenmodes at each $k_\theta$ which could balance the non-linear energy transfer, as has recently been shown for predominantly electrostatic turbulence.[59,60] Of course, the damping could also occur over the entire $k_\theta$ spectrum of damped modes. A similar comprehensive analysis similar to Refs. 59 and 60 would be required to better understand the saturation mechanism of the microtearing turbulence.

This effect appears to be amplified in the higher resolution case where the ~25% increase in transport occurs around the peak at $k_\theta \rho_s \sim 0.2$, with a small reduction at higher $k_\theta$. In either case, the spectrum tail decays very slowly and it's possible the simulations are missing some non-negligible fraction of transport. Additionally, because of the non-linear coupling, it is likely important to obtain the appropriate strength of the high-$k_\theta$ growth rates which will be increased slightly with refined $\Delta x$ (Fig. 1). Ultimately, more expensive runs are required to test for quantitative convergence at higher resolution.

### D. Stochasticity

Transport from microtearing modes is expected to be large when small scale islands grow sufficiently large to overlap, leading to stochasticity and the destruction of magnetic surfaces. We find this picture holds for the microtearing simulations, as illustrated in Fig. 6. Poincare surface-of-section plots are constructed by integrating each of 100 perturbed field line trajectories a total of 3000 poloidal transits using the simulated magnetic perturbations at every time (i.e., assuming $\delta B$ is fixed).[61,62] In the late-linear phase ($t = 25\ a/c_s$), only the highest $k_\theta$ modes are large enough to satisfy the overlap criteria ($w_{island} > \delta r_{rat}$). As a result, the magnetic surfaces are only slightly perturbed from the equilibrium, which would look like straight vertical lines in flux coordinates as plotted.

Early in the non-linear phase ($t = 50\ a/c_s$), half of the modes satisfy overlap and the surfaces are now almost

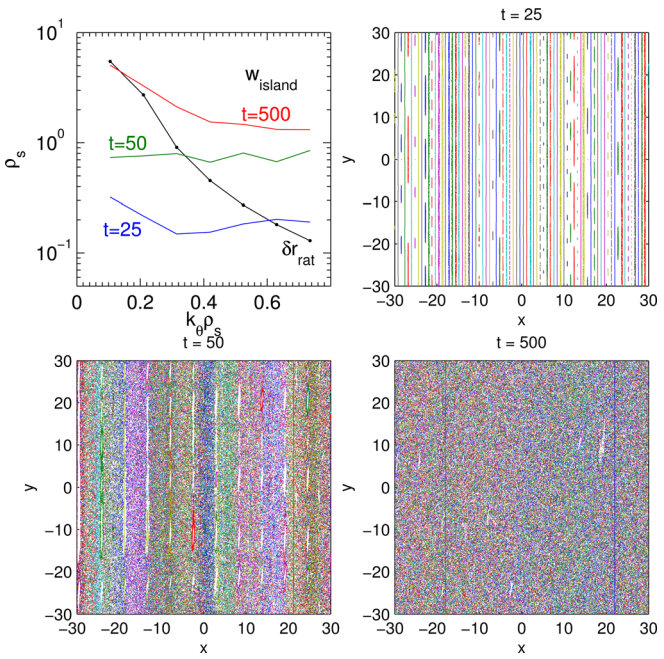


FIG. 6. (Color online) (a) Minimum separation in rational surfaces ($\delta r_{rat}$) and estimate of island widths ($w_{island}$) using $\delta B/B$ at three times in the simulation. (b)–(d) Poincare surface-of-section plots at the same three times using 100 field line trajectories each integrated 3000 poloidal transits.

completely destroyed, illustrated by broad stochastic regions with small islands of stability remaining around the lowest order rational surfaces. Well into the saturated phase ($t = 500\ a/c_s$), the field lines are globally stochastic. At this instant in time all but the lowest finite-$k_\theta$ mode satisfy island overlap.

A magnetic diffusivity is calculated directly from an ensemble average of the $N = 100$ field lines, $r_i(\ell)$, integrated along their trajectories $\ell$ (Refs. 61 and 62)

$$D_m = \frac{1}{N}\sum_{i=1}^{N}\lim_{\ell\to\infty}\frac{[r_i(\ell) - r_i(0)]^2}{2\ell} \qquad (2)$$

giving a time-averaged value $D_m \sim 6\times10^{-7}$ m in the saturated phase. Using the rms value for $\delta B/B_0 = 1.5\times10^{-3}$ and the relation $D_m = |\delta B/B|^2 L_c$,[33] the field line correlation length $L_c \sim 0.25$ m is much shorter than the electron mean free path ($\lambda_{mfp} \sim 12.5$ m). The corresponding collisionless ($L_c < \lambda_{mfp}$) test-particle stochastic transport model[33] $\chi_{e,RR} = D_m v_{Te} \approx 1.0\rho_s^2 c_s/a$ is within ~25% of the simulation (where we have neglected order unity coefficients), consistent with the transport being dominated by electrons diffusing in a stochastic magnetic field.

Previous modeling of an NSTX discharge unstable to microtearing modes[34,35] used the collisional Rechester-Rosenbluth stochastic transport model. In the absence of nonlinear simulations, the quasi-linear estimate for the saturated amplitude, $\delta B/B \approx \rho_e/L_{Te}$,[20] predicted $\chi_{e,RR} \sim 50$–$100\%$ smaller than experimental values. In the non-linear simulation above $\delta B/B \sim 0.15\%$ is about two times larger than $\rho_e/L_{Te} = 0.065\%$, so that using a larger saturated $\delta B/B$ as found here would provide an overestimate, bracketing the experimental values, reinforcing the conclusions in Refs. 34 and 35. However, the scaling of either collisional or collisionless Rechester-Rosenbluth estimates with this quasi-linear saturation rule is incapable of reproducing the predictions from nonlinear simulations, as discussed next.

## IV. TRANSPORT PARAMETRIC DEPENDENCIES

To make a comparison with experimental transport and confinement observations, the smaller computational domain (R1, Table II) was used to run numerous nonlinear simulations varying electron collision frequency ($\nu_{ei}$), temperature gradient ($a/L_{Te}$), beta ($\beta_e$), and $E\times B$ shearing rate ($\gamma_E$). Except for the $\gamma_E$ scan, all simulations did not include $E\times B$ shear ($\gamma_E = 0$).

### A. Electron collisionality

Fig. 7 shows the predicted transport $\chi_e$ (normalized to the gyroBohm value) as electron collision frequency is varied from 0.05-2× the experimental value (using $Z_{eff} = 2.9$). Over more than an order of magnitude (note the log-log axes), the predicted transport scales almost linearly with collision frequency, $\chi_e/(\rho_s^2 c_s/a) \sim (\nu_{ei}\, a/c_s)^{1.1} \sim \nu_{*e}^{1.1}$. This trend is qualitatively consistent with, although stronger than, the scaling of the linear growth rates which vary by only a factor of ~3–4 over the same range in collisionality.[11]

Assuming a direct relation between local transport and global confinement, $\tau_E \sim a^2/\chi_e$, Fig. 7 implies a confinement time that, for fixed $\rho_*$ and $\beta$, should scale similar to those deduced from dedicated dimensionless scaling experiments in both NSTX[36–38] and MAST,[39,40] $(\Omega_i\tau_E) \sim \nu_{*e}^{-(0.8-0.95)}$. Assuming this overly simplistic relation between local transport at one radius and global confinement obviously ignores many potentially important effects such as the variation in profiles and possible scaling of pedestal height with collisionality. Nevertheless, the magnitude and scaling of the predicted transport with collision frequency provides some evidence that the microtearing mode may in fact be an important component in describing transport and confinement scaling in these NBI heated NSTX and MAST discharges.

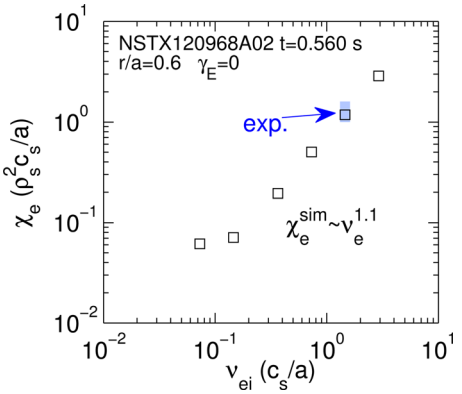


FIG. 7. (Color online) Normalized electron thermal diffusivity vs. normalized electron collision frequency (log-log scale). The shaded region shows the experimental values with uncertainties.

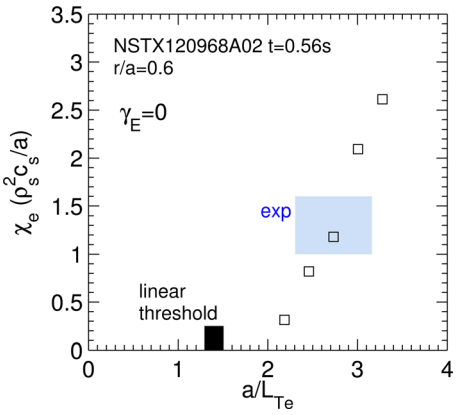


FIG. 8. (Color online) Electron thermal diffusivity vs. electron temperature gradient. The shaded region shows the experimental values with uncertainties.

### B. Electron temperature gradient

As found in multiple linear studies in both slab and toroidal geometry, the microtearing mode exhibits a threshold in electron temperature gradient. Non-linear simulations above the linear threshold show the predicted transport is very "stiff," with $\chi_e$ varying +/−100% for +/−20% change in $a/L_{Te}$ (Fig. 8). Such stiffness implies that profiles should adjust to be near marginal stability. It could therefore be just as important to characterize the scaling of the threshold with collisionality, complicating the simple $\nu_*$ scaling interpretation discussed above. Additionally, there appears to be an effective non-linear threshold ($a/L_{Te,NL} \approx 2.1$), that is ~40% larger than the linear threshold ($a/L_{Te,NL} \approx 1.5$), reminiscent of the so-called "Dimits shift" in ITG turbulence.[63] Such a strong upshift has been observed before in finite−$\beta$ ($\beta_e \leq 1\%$) simulations of ITG turbulence,[55,56] although the reason for this remains unclear.

### C. Electron beta

Fig. 9 shows that the non-linear transport is significant when electron beta is above the linear threshold, which for this case occurs at $\beta_e \approx 3.0\%$.[11] Similar to the $a/L_{Te}$ scan in Fig. 8, there appears to be an upshift in the nonlinear $\beta_e$ threshold (between 4.5 and 7%). Above this threshold, the transport roughly doubles over the range $\beta_e \approx$ 7–13% (0.8 – 1.5 × $\beta_{e,exp}$). While this is qualitatively consistent with

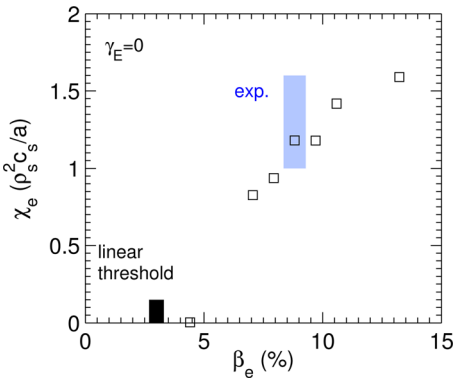


FIG. 9. (Color online) Electron thermal diffusivity vs. electron beta. The shaded region shows the experimental values with uncertainties.

NSTX and MAST experimental results,[36,40] the degradation is much stronger than the experimentally determined scaling exponent, $(B_T\tau_E) \sim \beta_e^{-0.1}$.

In all the above scans, the transport predictions qualitatively follow the linear stability analysis.[11] As mentioned in the Introduction, the test-particle stochastic transport models, coupled with the quasi-linear saturation estimate $\delta B/B \approx \rho_e/L_{Te}$, are unable to reproduce this behavior. To illustrate this, we write the Rechester-Rosenbluth[33] electron thermal diffusivity $\chi_e^{RR} \approx D_m v_{Te} = |\delta B/B|^2 L_c v_{Te}$ normalized by the gyro-Bohm diffusivity $(\rho_s^2 c_s/a)$ for both collisionless ($L_c = qR$ for $\lambda_{MFP} > qR$) and collisional ($L_c = \lambda_{MFP}$ for $\lambda_{MFP} < qR$) cases as:

$$\frac{\chi_e^{RR}}{\rho_s^2 c_s/a} = \min\left[1, \frac{1}{\varepsilon^{3/2}\nu_{*e}}\right]\frac{1}{\mu}\frac{qR}{a}\left(\frac{a}{L_{Te}}\right)^2,$$

where $\mu = (m_i/m_e)^{1/2}$, $\varepsilon = a/R$, $\nu_{*e} = \nu_{ei}\cdot qR/\varepsilon^{3/2}v_{Te}$, and $\min[1, 1/\varepsilon^{3/2}\nu_{*e}]$ represents the two limits. From this expression, we see the model does predict a nonlinear dependence of transport with $a/L_{Te}$. However, it does not know about the threshold behavior in $a/L_{Te}$ and $\beta_e$, the scaling with $\beta_e$, and if anything predicts a $\nu_*$ scaling opposite to that found from the non-linear simulations. Therefore, the non-linear simulations are critical for predicting trends in microtearing transport.

### D. ExB shear

The above simulations were run with E × B shear set to zero ($\gamma_E = 0$). However, as shown in Table I, the local E × B shearing rate ($\gamma_E = 0.17\ c_s/a$) is comparable to the maximum linear growth rate ($\gamma_{lin,max} = 0.15\ c_s/a$ for the non-linear simulation resolution, Fig. 1). It has been found in nonlinear simulations that such large E × B shear ($\gamma_E/\gamma_{lin,max} \sim 1$) can suppress ITG/TEM,[64] and even ETG[65,66] turbulence, and we find the same to hold true for these NSTX microtearing simulations. Fig. 10 shows that as $\gamma_E$ is increased from zero to the local experimental value, the predicted transport is reduced dramatically, which is no longer consistent with the local experimental $\chi_e$. Given the sensitivity of predicted transport with temperature gradient, an additional set of simulations was run with $a/L_{Te}$ increased 20%. The transport with experimental $\gamma_E$ is increased but remains ~3× smaller than the experimental value.

We note that the non-linear microtearing simulations for conventional aspect ratio[49] are not suppressed by such strong values of E × B shear. The reason for this difference is under investigation, although the microtearing modes in Ref. 49 are unstable at much lower wavenumbers with a peak in transport around $k_\theta\rho_s \approx$ 0.06-0.1 compared to $k_\theta\rho_s \approx$ 0.2–0.25 for the NSTX case.

Because of the expense of these nonlinear simulations, it is an unfortunate reality that extensive quantitative convergence has yet to be demonstrated for the range of parameters studied. Considering the consequences of radial resolution on the linear growth rates (Fig. 1) and the slowly decaying tail in the transport spectra (Fig. 5), it is likely that the predicted transport at experimental $\gamma_E$ will increase for both smaller $\Delta x$ and larger $k_{\theta,max}$. Including an impurity (carbon)

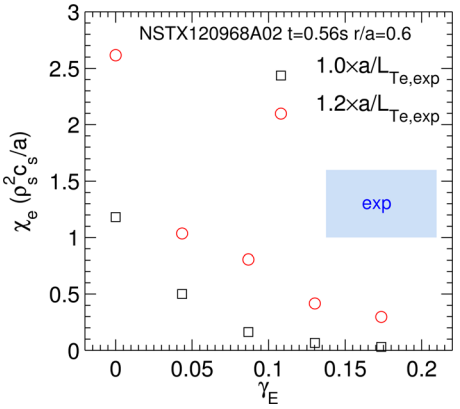


FIG. 10. (Color online) Electron thermal diffusivity vs. E×B shearing rate ($\gamma_E$, in units $c_s/a$). The shaded region shows the experimental values with uncertainties.

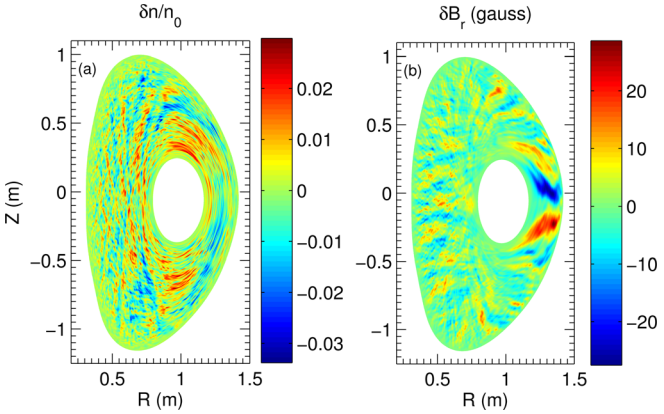


FIG. 11. (Color online) Snapshot of (a) normalized electron density perturbations and (b) $\delta B_r$ (in Gauss) in a (R,Z) toroidal plane.

ion consistent with experiment is also expected to increase the transport following the trend in the linear growth rates (Fig. 1).

As noted above, these simulations were run in the *local* limit which is valid only for asymptotically small $\rho_* = \rho_s/a \rightarrow 0$. At $r/a = 0.6$, in this NSTX discharge, $\rho_* \approx 1/130$, so that the simulated domain width ($L_x = 80\ \rho_s$) spans ~60% of the minor radius. However, in the local approximation simulations only use geometry and plasma parameters from the $r/a = 0.6$ surface. Linear analysis[11] shows that further out ($r/a = 0.7$–$0.8$), the microtearing mode can be more unstable and eventually a kinetic ballooning mode becomes unstable at $r/a \approx 0.8$. It is, therefore, possible that non-local effects could be important in determining the total transport. Such simulations will be yet more challenging if the microtearing resolution criteria $\Delta x \leq 1/(4k_{\theta,\max} s)$ must be satisfied at increasing magnetic shear towards the outer radii.

## V. REAL SPACE STRUCTURE AND MEASUREMENT OPPORTUNITIES

Although the strong experimental $E \times B$ shear reduces the predicted transport, we assume for now that the case which matches experimental transport ($\gamma_E = 0$) represents an upper limit to the level of turbulence to be expected.

To help illuminate possible diagnostic measurements of interest, we plot the density and radial magnetic field perturbations in laboratory coordinates (R,Z) at a toroidal cut in Fig. 11. In general, the nonlinear $\delta n$ and $\delta B_r$ features are qualitatively similar to the structure of the linear microtearing instability. The density perturbations are elongated poloidally but narrow radially and the strength of the $\delta n$ fluctuations is roughly uniform (statistically) around the poloidal circumference. In contrast to this, the magnetic perturbations ($\delta B_r$) are spatially broad on the outboard side and become finer scale on the inboard side. The $\delta B_r$ fluctuations are also much stronger on the outboard side with instantaneous values (~25–30 Gauss) approaching 1% of the local equilibrium field (~3.5 kG).

The recently implemented beam emission spectroscopy (BES) diagnostics[67] is sensitive to density fluctuations at the poloidal wavelengths relevant to microtearing turbulence ($k_\theta \rho_s < 1$). However, typical BES fiber optic views are 2–3 cm wide, and it is unknown how sensitive it will be to the narrow density perturbations. For example, the characteristic width of $\delta n$ in Fig. 11 is coupled in large part to $\Delta r_{rat}$ associated with the peak magnetic fluctuations at $n \sim 10$ or $\Delta r_{rat} \sim 2.8\rho_s \sim 1.3$ cm. The well established high-k scattering diagnostic[68] configured for $k_r > k_\theta$ might be also suitable for detecting density perturbations associated with microtearing modes. Future work will focus on correlating BES and high-k measurements with simulations using appropriate synthetic diagnostics in discharges expected to be unstable to the microtearing instability.

As microtearing turbulence is fundamentally magnetic in nature, there is great interest in directly measuring local magnetic perturbations. This has been attempted before in other tokamaks using cross polarization scattering (CPS).[69,70] However, the particular configuration implemented was sensitive mostly to magnetic perturbations with $k_\theta \rho_s \approx 0$ and $k_r \rho_s \gg 0$, which is not in alignment with the strongest microtearing perturbations shown in Fig. 11, where $k_\theta \rho_s \approx 0.2$ and $k_r \rho_s \approx 0$ (Figs. 4(c) and 4(d)).

Recently, a radial retro-reflecting polarimetry diagnostic has been proposed.[71] While this measurement is line-integrated, it may be sensitive to microtearing turbulence because of the strong, ballooning, broad $\delta B_r$ perturbations local to the outboard side. To test this, the simulated density and magnetic perturbations were used to calculate the expected polarimeter mixer phase for the $f = 288$ GHz system, directed across the magnetic axis. The simulations include both Faraday rotation and Cotton-Mouton effects along a 1D chord and therefore do not capture finite beam width effects.

Fig. 12 shows the predicted time response when using only the equilibrium field and density, along with two cases adding only the simulated density perturbations and both density and magnetic perturbations. The phase response owing to the radially narrow density perturbations is negligibly small compared to the contribution from the magnetic perturbations, which is as large as 1.5° peak-to-peak, or ~0.3° rms. This level is above the measured noise floor of the diagnostic[72] suggesting it may in fact be sensitive to magnetic fluctuations from microtearing turbulence. It should be cautioned that this

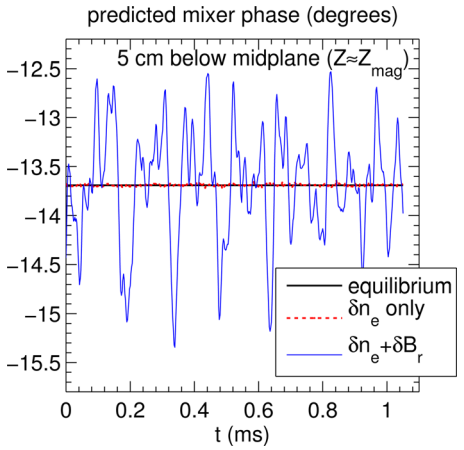


FIG. 12. (Color online) Theoretically predicted line-integrated polarimeter mixer phase using only the equilibrium field and density (thick black solid), equilibrium plus $\delta$n(R,Z,t) (red dashed), and equilibrium plus $\delta$n(R,Z,t) and $\delta B_r$(R,Z,t) (thin blue solid).

initial calculation does not account for other perturbations that are likely to be present in the plasma (MHD phenomena, neoclassical tearing modes, etc.) that could complicate interpretation from the actual measurement.

## VI. SUMMARY

Gyrokinetic simulations in a high-collisionality NSTX discharge find that microtearing modes are linearly unstable over a broad region of the plasma (r/a = 0.5–0.8). First local non-linear simulations have been performed for one flux surface (r/a = 0.6), which predict electron thermal transport is dominated by magnetic flutter and can be comparable to experimental values. The transport is shown to be consistent with electrons diffusing in a globally stochastic region, as found from integrating field line trajectories using the simulated magnetic perturbations. However, the test particle stochastic transport models do not reproduce the scaling predicted from non-linear simulations.

Most notably, in the absence of E × B shear, the transport is predicted to decrease with decreasing collisionality, $\chi_e/(\rho_s^2 c_s/a) \sim (\nu_{ei} a/c_s)^{1.1} \sim \nu_{*e}^{1.1}$, consistent both with linear growth rates and with the observed scaling of normalized energy confinement times from dedicated dimensionless scaling experiments, $(B_T \tau_E) \sim \nu_{*e}^{-(0.8-0.95)}$. However, the predicted transport is also very stiff with electron temperature gradient (and electron beta, to a less extent) suggesting it may be just as important to characterize the scaling of the microtearing threshold gradient. When including the experimental level of E × B shear, which is close to the maximum linear growth rate, the predicted transport is very small, no longer consistent with experimental transport analysis. A 20% increase in electron temperature gradient recovers a significant amount of transport but it remains ~3× smaller than experimental values.

While considerable care has been taken to ensure that the non-linear simulations are sufficiently resolved to at least qualitatively represent the physical nature of microtearing turbulence, a number of caveats remain that could alter the quantitative results. Limited convergence studies have been performed, although comprehensive quantitative convergence has yet to be demonstrated. These first nonlinear simulations also did not include an impurity carbon species that is measured experimentally. Linear analysis shows that growth rates increase when including a carbon species which would likely increase the predicted transport. Additionally, these simulations were run in the *local* limit but non-local effects (due to profile variations at large $\rho_*$) could influence the predicted results. Future non-linear simulations will continue to explore the influence of all these effects.

Finally, the characteristics of microtearing turbulence are seen to be quite distinct from other traditional core turbulence mechanisms. While the instability exists generally at poloidal scales of the ion gyroradius ($k_\theta \rho_s < 1$), density perturbation are very narrow ($<1\ \rho_s$) in the radial direction. In contrast, shear magnetic perturbations balloon to the outboard side where they are very broad. Using the predicted large local amplitude (approaching $\delta B/B \sim 1\%$ peak-to-peak on the outboard side) calculations indicate a planned polarimetry diagnostic may very well be sensitive to the magnetic perturbations from microtearing turbulence.

## ACKNOWLEDGMENTS

We are happy to thank the useful discussions with H. Doerk, S. P. Gerhardt, J. E. Menard, J. L. Peterson, and D. R. Smith. This research used resources of the National Energy Research Scientific Computing Center, supported by DOE Contract DE-AC02-05CH11231, and the Oak Ridge Leadership Computing Facility, supported by DOE contract DE-AC05-00OR22725. This work was also supported by DOE contracts DE-AC02-09CH11466, DE-FG03-95ER54309, DE-AC52-07NA27344, and DE-FG02-99ER54527.

[1]M. Kotschenreuther, W. Dorland, Q. P. Liu, M. C. Zarnstorff, R. L. Miller, and Y. R. Lin-Liu, Nucl. Fusion **40**, 677 (2000).
[2]H. R. Wilson, J.-W. Ahn, R. J. Akers, D. Applegate, R. A. Cairns, J. P. Christiansen, J. W. Connor, G. Counsell, A. Dnestrovskij, W. D. Dorland, M. J. Hole, N. Joiner, A. Kirk, P. J. Knight, C. N. Lashmore-Davies, K. G. McClements, D. E. McGregor, M. R. O'Brien, C. M. Roach, S. Tsaun, and G. M. Voss, Nucl. Fusion **44**, 917 (2004).
[3]D. J. Applegate, C. M. Roach, S. C. Cowley, W. D. Dorland, N. Joiner, R. J. Akers, N. J Conway, A. R. Field, A. Patel, M. Valovic, and M. J. Walsh, Phys. Plasmas **11**, 5085 (2004).
[4]C. M. Roach, D. J. Applegate, J. W. Connor, S. C. Cowley, W. D. Dorland, R. J. Hastie, N. Joiner, S. Saarelma, A. A. Schekochihin, R. J. Akers, C. Brickly, A. R. Field, M. Valovic, and the MAST team, Plasma Phys. Controlled Fusion **47**, B233 (2005).
[5]D. J. Applegate, C. M. Roach, J. W. Connor, S. C. Cowley, W. Dorland, R. J. Hastie, and N. Joiner, Plasma Phys. Controlled Fusion **49**, 1113 (2007).
[6]M. H. Redi, W. Dorland, R. Bell, P. Banoli, C. Bourdelle, J. Candy, D. Ernst, C. Fiore, D. Gates, G. Hammett, K. Hill, S. Kaye, B. LeBlanc, J. Menard, D. Mikkelsen, G. Rewoldt, J. Rice, R. Waltz, and S. Wukitch, paper presented at the 30st EPS Conference on Controlled Fusion and Plasma Physics (St. Petersburg), P-4.94, 2003.
[7]M. H. Redi, S. Kaye, W. Dorland, R. Bell, C. Bourdelle, S. Ethier, D. Gates, G. Hammett, K. Hill, B. LeBlanc, D. McCune, J. Menard, D. Mikkelsen, G. Rewoldt, and E. Synakowski, paper presented at the 31st EPS Conference on Controlled Fusion and Plasma Physics (London), P-2.162, 2004.
[8]M. H. Redi, W. Dorland, C. L. Fiore, D. Stutman, J. A. Baumgaertel, B. Davis, S. M. Kaye, D. C. McCune, J. Menard, and G. Rewoldt, paper presented at the 32nd EPS Conference on Controlled Fusion and Plasma Physics (Tarragona), P-5.041, 2005.

[9]F. M. Levinton, H. Yuh, M. G. Bell, R. E. Bell, L. Delgado-Aparicio, M. Finkenthal, E. D. Fredrickson, D. A. Gates, S. M. Kaye, B. P. LeBlanc, R. Maingi, J. E. Menard, D. Mikkelsen, D. Mueller, R. Raman, G. Rewoldt, S. A. Sabbagh, D. Stutman, K. Tritz, and W. Wang, Phys. Plasmas **14**, 056119 (2007).
[10]D. R. Smith, W. Guttenfelder, B. P. LeBlanc, and D. R. Mikkelsen, Plasma Phys. Controlled Fusion **53**, 035013 (2011).
[11]W. Guttenfelder, J. Candy, S. M. Kaye, W. M. Nevins, R. E. Bell, G. W. Hammett, B. P. LeBlanc, and H. Yuh, Phys. Plasmas **19**, 022506 (2012).
[12]L. Vermare, C. Angioni, A. Bottino, A. G. Peeters and the ASDEX Upgrade Team, J. Phys. Conf. Ser. **123**, 012040 (2008).
[13]D. Told, F. Jenko, P. Xanthopoulous, L. D. Horton, E. Wolfrum, and ASDEX Upgrade Team, Phys. Plasmas **15**, 102306 (2008).
[14]I. Predebon, F. Sattin, M. Veranda, D. Bonfiglio, and S. Cappello, Phys. Rev. Lett. **105**, 195001 (2010).
[15]H. P. Furth, J. Killen, and M. N. Rosenbluth, Phys. Fluids **6**, 459 (1963).
[16]H. P. Furth, P. H. Rutherford, and H. Selberg, Phys. Fluids **16**, 1054 (1973).
[17]J. Wesson, *Tokamaks* (Oxford University Press, New York, 2004).
[18]R. D. Hazeltine, D. Dobrott, and T. S. Wang, Phys. Fluids **18**, 1778 (1975).
[19]J. F. Drake and Y. C. Lee, Phys. Fluids **20**, 1341 (1977).
[20]J. F. Drake, N. T. Gladd, C. S. Liu, and C. L. Chang, Phys. Rev. Lett. **44**, 994 (1980).
[21]M. Rosenberg, R. R. Dominguez, W. Pfeiffer, and R. E. Waltz, Phys. Fluids **23**, 2022 (1980).
[22]N. T. Gladd, J. F. Drake, C. L. Chang, and C. S. Liu, Phys. Fluids **23**, 1182 (1980).
[23]D'Ippolito, Y. C. Lee, and J. F. Drake, Phys. Fluids **23**, 771 (1980).
[24]R. R. Dominguez, M. Rosenberg, and C. S. Chang, Phys. Fluids **24**, 472 (1981).
[25]C. S. Chang, R. R. Dominguez, and R. D. Hazeltine, Phys. Fluids **24**, 1655 (1981).
[26]A. B. Hassam, Phys. Fluids **23**, 38 (1980).
[27]A. B. Hassam, Phys. Fluids **23**, 2493 (1980).
[28]G. G. Craddock and P. W. Terry, Phys. Fluids B **3**, 3286 (1991).
[29]L. Chen, P. H. Rutherford, and W. M. Tang, Phys. Rev. Lett. **39**, 460 (1977).
[30]P. J. Catto and M. N. Rosenbluth, Phys. Fluids **24**, 243 (1981).
[31]J. W. Connor, S. C. Cowley, and R. J. Hastie, Plasma Physics Controlled Fusion **32**, 799 (1990).
[32]G. M. Zaslavsky and B. V. Chirikov, Sov. Phys. Usp. **14**, 549 (1972).
[33]A. B. Rechester and M. N. Rosenbluth, Phys. Rev. Lett. **40**, 38 (1978).
[34]K. L. Wong, S. Kaye, D. R. Mikkelsen, J. A. Krommes, K. Hill, R. Bell, and B. LeBlanc, Phys. Rev. Lett. **99**, 135003 (2007).
[35]K. L. Wong, S. Kaye, D. R. Mikkelsen, J. A. Krommes, K. Hill, R. Bell, and B. LeBlanc, Phys. Plasmas **15**, 056108 (2008).
[36]S. M. Kaye, F. M. Levinton, D. Stutman, K. Tritz, H. Yuh, M. G. Bell, R. E. Bell, C. W. Domier, D. Gates, W. Horton, J. Kim, B. P. LeBlanc, N. C. Luhmann Jr., R. Maingi, E. Mazzucato, J. E. Menard, D. Mikkelsen, D. Mueller, H. Park, G. Rewoldt, S. A. Sabbagh, D. R. Smith, and W. Wang, Nucl. Fusion **47**, 499 (2007).
[37]S. M. Kaye, R. E. Bell, D. Gates, B. P. LeBlanc, F. M. Levinton, J. E. Menard, D. Mueller, G. Rewoldt, S. A. Sabbagh, W. Wang, and H. Yuh, Phys. Rev. Lett **98**, 175002 (2007).
[38]S. M. Kaye, S. P. Gerhardt, R. Maingi, R. E. Bell, A. Diallo, B. P. LeBlanc, Bull. Am. Phys. Soc. **56**, 249 (2011) http://meetings.aps.org/link/BAPS.2011.DPP.PP9.30.
[39]M. Valovič, R. Akers, M. de Bock, J. McCone, L. Garzotti, C. Michael, G. Naylor, A. Patel, C. M. Roach, R. Scannell, M. Turnyanskiy, M. Wisse, W. Guttenfelder, J. Candy, and the MAST team, Nucl. Fusion **51**, 073045 (2011).
[40]M. Valovič, R. Akers, G. Cunningham, L. Garzotti, B. Lloyd, D. Muir, A. Patel, D. Taylor, M. Turnyanskiy, M. Walsh, and the MAST team, Nucl. Fusion **49**, 075016 (2009).
[41]S. P. Gerhardt, D. A. Gates, S. M. Kaye, R. Maingi, J. E. Menard, S. A. Sabbagh, V. Soukhanovskii, M. G. Bell, R. E. Bell, J. M Canik, E. Fredrickson, R. Kaita, E. Kolemen, H. Kugel, B. P. LeBlanc, D. Mastrovito, D. Mueller, and H. Yuh, Nucl. Fusion **51**, 073031 (2011).
[42]J. E. Menard, M. Bell, J. Bialek, J. Canik, J. Chrzanowski, M. Denault, L. Dudek, D. A. Gates, S. Gerhardt, W. Guttenfelder, R. Hatcher, R. Kaita, S. Kaye, C. Kessel, E. Kolemen, H. Kugel, R. Maingi, M. Mardenfeld, D. Mueller, B. Nelson, C. Neumeyer, M. Ono, E. Perry, R. Ramakrishnan, R. Raman, S. Sabbagh, M. Smith, V. Soukhanovskii, T. Stevenson, R. Strykowsky, P. Titus, K. Tresemer, M. Viola, M. Williams, R. Woolley, A. Zolfaghari, and the NSTX Team, Nucl. Fusion (Submitted).
[43]C. C. Petty, Phys. Plasmas **15**, 080501 (2008).
[44]D. Applegate, Ph.D. thesis, Imperial College London, 2006.
[45]M. Kotschenreuther, G. Rewoldt, and W. M. Tang, Comp. Phys. Comm. **88**, 128 (1995).
[46]W. Dorland, F. Jenko, M. Kotschenreuther, and B. N. Rogers, Phys. Rev. Lett. **85**, 5579 (2000).
[47]B. D. Scott, Plasma Phys. Controlled Fusion **45**, A385 (2003).
[48]W. Guttenfelder, J. Candy, S. M. Kaye, W. M. Nevins, E. Wang, R. E. Bell, G. W. Hammett, B. P. LeBlanc, D. R. Mikkelsen, and H. Yuh, Phys. Rev. Lett. **106**, 155004 (2011).
[49]H. Doerk, F. Jenko, M. J. Pueschel, and D. R. Hatch, Phys. Rev. Lett. **102**, 155003 (2011); H. Doerk, F. Jenko, T. Gorler, D. Told, M. J. Pueschel, D. R. Hatch, Phys. Plasmas **19**, 055907 (2012).
[50]J. Candy and R. E. Waltz, Phys. Rev. Lett. **91**, 045001 (2003).
[51]J. Candy and R. E. Waltz, J. Comput. Phys. **186**, 545 (2003).
[52]J. Candy, Plasma Phys. Controlled Fusion **51**, 105009 (2009).
[53]J. Candy and E. Belli, General Atomics Technical Report No. GA-A26818 (2010).
[54]R. J. Hawryluk, in *Proceedings of the Course on Physics of Plasmas Close to Thermonuclear Conditions, Varenna* (1979), Vol. 1, p 19.
[55]M. J. Pueschel, M. Kammerer and F. Jenko, Phys. Plasmas **15**, 102310 (2008).
[56]M. J. Pueschel and F. Jenko, Phys. Plasmas **17**, 062307 (2010).
[57]F. Jenko and W. Dorland, Plasma Phys. Controlled Fusion **43**, A141 (2001).
[58]J. Candy, Phys. Plasmas **12**, 072307 (2005).
[59]D. R. Hatch, P. W. Terry, F. Jenko, F. Merz, and W. M. Nevins, Phys. Rev. Lett. **106**, 115003 (2011).
[60]D. R. Hatch, P. W. Terry, F. Jenko, F. Merz, M. J. Pueschel, W. M. Nevins, and E. Wang, Phys. Plasmas **18**, 055706 (2011).
[61]E. Wang, W. M. Nevins, J. Candy, D. Hatch, P. Terry, and W. Guttenfelder, Phys. Plasmas **18**, 056111 (2011).
[62]W. M. Nevins, E. Wang, and J. Candy, Phys. Rev. Lett **106**, 065003 (2011).
[63]A. M. Dimits, G. Bateman, M. A. Beer, B. I. Cohen, W. Dorland, G. W. Hammett, C. Kim, J. E. Kinsey, M. Kotschenreuther, A. H. Kritz, L. L. Lao, J. Mandrekas, W. M. Nevins, S. E. Parker, A. J. Redd, D. E. Shumaker, R. Sydora, and J. Weiland, Phys. Plasmas **7**, 969 (2000).
[64]J. E. Kinsey, R. E. Waltz, and J. Candy, Phys. Plasmas **14**, 102306 (2007).
[65]C. M. Roach, I. G. Abel, R. J. Akers, W. Arter, M. Barnes, Y. Camenen, F. J. Casson, G. Colyer, J. W. Connor, S. C. Cowley, D. Dickinson, W. Dorland, A. R. Field, W. Guttenfelder, G. W. Hammett, R. J. Hastie, E. Highcock, N. F. Loureiro, A. G. Peeters, M. Reshko, S. Saarelma, A. A. Schekochihin, M. Valovic, and H. R. Wilson, Plasma Phys. Controlled Fusion **51**, 124020 (2009).
[66]W. Guttenfelder and J. Candy, Phys. Plasmas **18**, 022506 (2011).
[67]D. R. Smith, H. Feder, R. Feder, R. J. Fonck, G. Labik, G. R. McKee, N. Schoenbeck, B. C. Stratton, I. Uzon-Kaymak, G. Winz, Rev. Sci. Instrum **81**, 10D717 (2010).
[68]D. R. Smith, E. Mazzucato, W. Lee, H. K. Park, C. W. Domier, and N. C. Luhmann, Jr., Rev. Sci. Instrum **79**, 123501 (2008).
[69]X. L. Zou, L. Colas, M. Paume, J. M. Chareau, L. Laurent, P. Devynck, and D. Gresillon, Phys. Rev. Lett. **75**, 1090 (1995).
[70]L. Colas, X. L. Zou, M. Paume, J. M. Chareau, L. Guiziou, G. T. Hoang, Y. Michelot, and D. Gresillon, Nucl. Fusion **38**, 903 (1998).
[71]J. Zhang, N. A. Crocker, T. A. Carter, S. Kubota, and W. A. Peebles, Rev. Sci. Instrum. **81**, 10D519 (2010).
[72]J. Zhang, W. A. Peebles, N. A. Crocker, T. L. Rhodes, E. J. Doyle, T. A. Carter, L. Zeng, S. Kubota, and W. Guttenfelder, Bull. Am. Phys. Soc. **56**, 257 (2011) http://meetings.aps.org/link/BAPS.2011.DPP.PP9.71.